CORROSION SCIENCE AND TECHNOLOGY, Vol.24, No.5(2025), pp.319~326 pISSN 1598-6462 / eISSN 2288-6524
[Research Paper] DOI: https://doi.org/10.14773/cst.2025.24.5.319

Pitting Morphology and Electrochemical Characteristics of 304 Stainless Steel Subjected to High-Temperature Exposure under Salt Spray Conditions

Ji-Hyeon Kim, Ju-Been Ham, Sae-Deok Seo, SeoWoo Nam, Hee-Chang Seo, and Young-Cheon Kim†

School of Materials Science & Engineering, Research Center for Energy and Clean Technology, Gyeongkuk National University, Andong-si, 36729, Korea

(Received June 22, 2025; Revised July 14, 2025; Accepted July 21, 2025)

Stainless steel (STS), which contains over 10.5 wt% chromium (Cr), forms a passive film in various environments, providing superior corrosion resistance compared to conventional steels. However, exposure to marine atmospheric conditions and prolonged high temperatures can compromise the protective function of this passive film, leading to pitting corrosion. This study investigates the pitting behavior and corrosion characteristics of STS304 specimens using salt spray testing (SST) and electrochemical analysis. SST was conducted on both as-received STS304 specimens and those subjected to high-temperature exposure (H_STS304), with cumulative exposure durations of 200, 300, 400, and 500 hours in 100-hour intervals. Analysis of the 3D surface profiles revealed that the frequency and size of pitting corrosion increased with longer salt spray exposure times, a trend that became more pronounced after high-temperature exposure. Additionally, H_STS304 exhibited a less stable passive region during polarization tests and showed significant potential fluctuations in open circuit potential (OCP) measurements.

Keywords: *STS 304, Salt Spray Test, Pitting morphology, Corrosion potential, Passive film*

1. Introduction

Austenitic stainless steel, a Cr-Ni based alloy primarily composed of chromium (Cr) and nickel (Ni), possesses excellent corrosion resistance, mechanical strength, and formability. Owing to these properties, stainless steel is widely used in various industries such as chemical, marine, and food processing industries [1-3]. Additionally, its high thermal conductivity makes it a suitable material for heat exchangers exposed to high-temperature and high-humidity environments, including chemical process piping and storage tanks [4,5].

However, the superior properties of STS 304 can degrade when exposed to elevated temperatures. Particularly within the sensitization range of 550 ~ 800 ºC, chromium and carbon in the alloy may form chromium carbides ($Cr_{23}C_6$) along grain boundaries, resulting in chromium depletion [6-9]. This phenomenon is a major cause of corrosion resistance degradation [10,11], leading to localized corrosion forms such as intergranular corrosion (IGC), intergranular stress corrosion cracking (IGSCC), and pitting corrosion. When exposed to saline environments, chloride ions (Cl^-) can penetrate the metal surface, disrupt the passive film, and promote pitting by forming metal chlorides [12-15].

To mitigate localized corrosion, solution heat treatment (SHT) is often applied to dissolve chromium-depleted zones [16,17]. Furthermore, the addition of stabilizing elements such as niobium (Nb) and titanium (Ti) has been investigated to suppress carbide precipitation and improve resistance to intergranular corrosion by preventing chromium depletion at grain boundaries [18-20]. Recent studies also aim to elucidate the influence of microstructural changes induced by high-temperature exposure on corrosion behavior and to quantitatively analyze the relationship between microstructural stability and corrosion resistance [21-23].

Although several studies have qualitatively investigated the microstructural changes of STS 304 under high-

†Corresponding author: yckim@gknu.ac.kr
Ji-Hyeon Kim: Graduate Student, Ju-Been Ham: Graduate Student, Sae-Deok Seo: Graduate Student, Seo-Woo Nam: Graduate Student, Hee-Chang Seo: Graduate Student, Young-Cheon Kim: Professor

temperature exposure and their effects on corrosion behavior, quantitative assessments of localized corrosion in chloride-containing environments remain limited [24,25]. Some attempts have been made to analyze the relationship between pit morphology and electrochemical characteristics. However, systematic investigations that incorporate thermal degradation effects are still lacking. Therefore, further studies are required to quantitatively establish the correlation between microstructural stability and corrosion resistance of STS 304 after high-temperature exposure. In this study, the localized corrosion behavior of STS 304 after high-temperature exposure was quantitatively investigated. To simulate chloride-rich service environments, salt spray testing (SST) was conducted, and pit morphology was characterized using a 3D confocal laser scanning microscope. Additionally, open circuit potential (OCP) and polarization tests were performed to analyze the correlation between electrochemical behavior and corrosion resistance.

2. Experimental Methods

2.1 Specimen

The alloy specimens used in this study were austenitic stainless steel STS 304, and their chemical composition is presented in Table 1. The specimens were prepared in the form of thin films with dimensions of 100 mm × 24 mm and a thickness of 0.05 mm as shown in Fig. 1a. Surface roughness analysis was performed using an AFM (NX10, Park Systems, Korea) and a 3D confocal microscope (VK-X3000, Keyence, Japan) at Gyeongkuk National University, and the average roughness (Ra) was measured to be 4–7 μm. Specimens that had been exposed to high temperatures were designated as H_STS 304, while those without such exposure were referred to as STS 304.

2.2 Salt Spray Test

To evaluate the corrosion resistance of the metal, a salt spray test was conducted to simulate the corrosion mechanism in a seawater-like environment. The appearance of the specimens after testing is shown in Fig. 1b. The test conditions were established based on relevant standards, including ASTM B117, ISO 9227, and KS D9502 [26]. The test was performed using a 5 wt% NaCl aqueous solution under the conditions listed in Table 2. The corrosion characteristics of the specimens were evaluated at cumulative exposure times of 200, 300, 400, and 500 hours.

2.3 Electrochemical Corrosion Test

To investigate the electrochemical characteristics, anodic polarization tests and open circuit potential (OCP) measurements were performed. Each specimen was prepared by attaching a shielded copper wire to the

Fig. 1. The specimen (a) before and (b) after the salt spray test

Table 2. Conditions of the cyclic salt spray test

Step	Mode	Time
1	35 °C, 5 wt% NaCl spray, 35% RH	2 hours
2	70 °C, 30% RH (Dry condition)	2 hours
3	50 °C, 95% RH (Humid condition)	2 hours
One cycle (Step 1 + Step 2 + Step 3)		6 hours
Total test time: 200, 300, 400, 500 hours		

Table 1. Chemical composition of Stainless steel 304 (wt%)

Composition	C	Si	Mn	P	S	Cr	Ni	Fe
wt%	0.08	1	2	0.045	0.03	18-20	8-10.5	Bal.

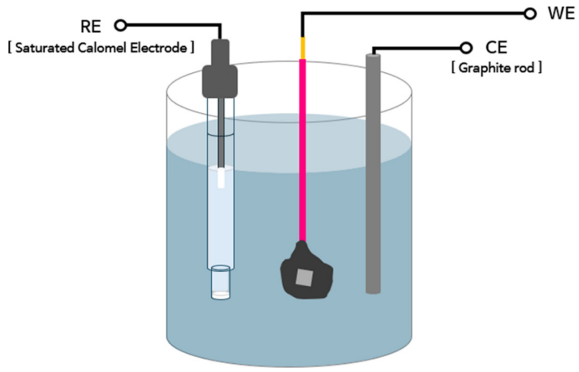

Fig. 2. Schematic illustration of the three-electrode electrochemical measurement system

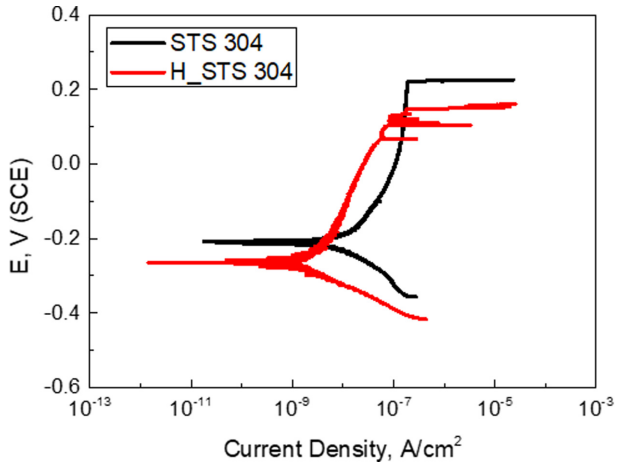

Fig. 3. Anodic polarization curves of STS 304 and H_STS 304 in 5 wt% NaCl solution

Table 3. Comparison of Ecorr and Epit for STS 304 and H_STS 304 in 5 wt% NaCl solution

Specimen	Ecorr, V (SCE)	Epit, V (SCE)
STS 304	-0.211	0.222
H_STS 304	-0.265	0.148

backside using carbon tape and embedding it in epoxy resin, exposing only a 0.25 cm^2 surface area. A 5 wt% NaCl aqueous solution (40.4 g of NaCl in 800 mL of distilled water) was used as an electrolyte. A saturated calomel electrode (SCE) served as the reference electrode, and a high-density graphite rod was used as the counter electrode. The configuration of the three-electrode system is shown in Fig. 2. The solution temperature was maintained at room temperature (25 ± 1 ºC), and dissolved oxygen was removed by purging with N_2 gas at a flow rate of 250 mL/min for 30 minutes. The polarization test was carried out by applying a potential sweep from -200 mV relative to the corrosion potential at a scan rate of 3.333 mV/s, and the test was terminated upon reaching the pitting potential. The OCP test was conducted for 20 hours under open circuit conditions to monitor the variation in corrosion potential. Both tests were performed under identical conditions using a multichannel electrochemical workstation (ZIVE MP1, WonATech, Korea).

2.4 Measurement of 3D surface profile

To quantitatively analyze the pit morphology of STS 304 and H_STS 304 specimens as a function of salt spray exposure time, the pit depth and width were measured using a 3D confocal laser scanning microscope (VK-X3000, Keyence, Japan). Four specimens were prepared for each exposure duration. From each specimen, 10 representative pits were randomly selected from the central region, resulting in a total of 40 measurement points per time condition. These pit dimensions were quantitatively analyzed and subsequently used for statistical comparison. As the edge regions of specimens during salt spray testing are known to promote solution accumulation [27,28], measurements were performed primarily in the central region, at least 1 cm inward from the edges, to minimize distortion.

3. Results and Discussion

Fig. 3 shows the polarization curves of STS 304 and H_STS 304 specimens in a 5 wt% NaCl solution. The experiment was terminated upon reaching the pitting potential. Both specimens exhibited the typical active-passive transition behavior of austenitic stainless steel, with the formation of a passive region beyond a certain potential. Table 3 summarizes the corrosion potential (E_{corr}) and pitting potential (E_{pit}) obtained using the Tafel extrapolation method. H_STS 304 exhibited a lower E_{corr} of -0.265 V_{SCE} and E_{pit} of 0.148 V_{SCE}, compared to -0.211 V_{SCE} and 0.222 V_{SCE}, respectively, for STS 304. This corresponds to reductions of 0.054 V_{SCE} and 0.074 V_{SCE}. These results suggest a decrease in the overall corrosion resistance of the H_STS 304 specimen [29,30]. Additionally, the H_STS 304 specimen exhibited a gradual increase in current density within the same potential range of the passive region, and the overall

passive potential range was relatively narrower than that of STS 304.

Fig. 4 shows the open circuit potential (OCP) measurements of STS 304 and H_STS 304 specimens in a 5 wt% NaCl solution over a period of 20 hours. Immediately after the start of the measurement, both specimens exhibited a sharp ennoblement in potential, which is attributed to the rapid formation of a passive film [31]. The potential of STS 304 stabilized around -0.222 V_{SCE}, with a maximum potential of -0.156 V_{SCE}. In contrast, the H_STS 304 specimen exhibited a more noble maximum potential of -0.086 V_{SCE} compared to STS 304, suggesting apparently higher corrosion resistance in the electrolyte environment. However, its potential failed to stabilize and exhibited repeated irregular fluctuations. These results indicate that the passive film formed on the surface of the H_STS 304 specimen was less stable. The potential oscillations are presumed to be caused by non-uniform formation of the passive film, or by the repeated processes of local breakdown and re-passivation [32,33]. This phenomenon has been widely reported to occur within the temperature range of 550 ~ 800 ℃, and the high-temperature exposure condition in this study is suggested to have contributed to such behavior [34].

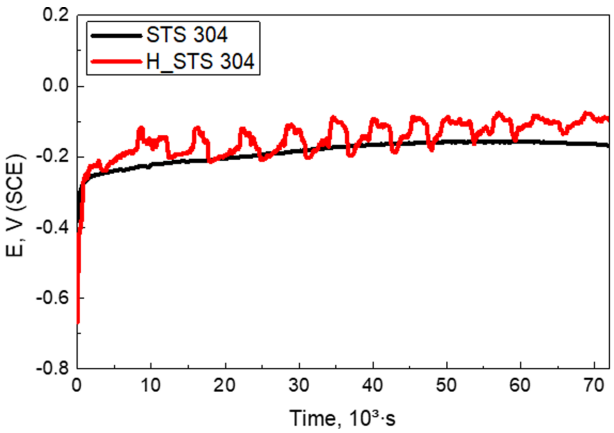

Fig. 4. Open circuit potential (OCP) curves of STS 304 and H_STS 304 in 5 wt% NaCl solution

Although overall corrosion severity can be assessed by measuring the weight loss caused by localized pitting, it

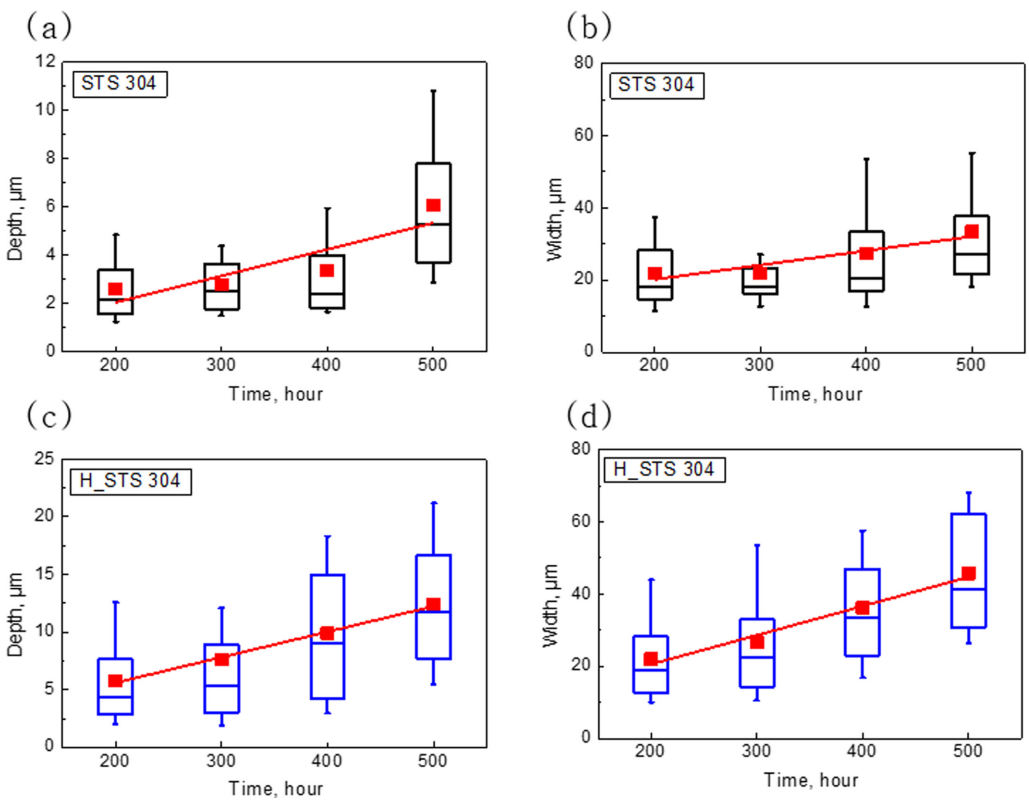

Fig. 5. Comparison of pit depth and width evolution in STS 304 and H_STS 304 after salt spray testing; (a) STS 304 depth; (b) STS 304 width; (c) H_STS 304 depth; (d) H_STS 304 width

is inherently difficult to quantitatively evaluate the distribution and severity of damage due to the localized nature of pitting corrosion. Therefore, in this study, the pit depth and width of STS 304 and H_STS 304 specimens were quantitatively measured using a 3D confocal laser scanning microscope as a function of salt spray exposure time. The analysis was conducted by categorizing the specimens into four groups for each material, corresponding to exposure durations of 200, 300, 400, and 500 hours. The measured pit depths and widths were visualized using box plots, and 3D surface images were additionally employed to enhance the understanding of pit distribution characteristics.

Fig. 5 presents the statistical distribution of pit depth and width over time. The box represents the interquartile range from the 25th to 75th percentiles, the internal horizontal line indicates the median, the whiskers extend from the 10th to 90th percentiles, and the red symbols denote the mean value. The average values of pit size according to exposure time are summarized in Table 4, and linear trendlines were added to clarify the progression trend. The results showed a gradual increase in both pit depth and width over time for both specimen types. In particular, the H_STS 304 specimens exhibited larger average pit sizes and a broader distribution in both the box and whisker ranges, indicating greater variability in pit dimensions. This suggests that pitting did not occur uniformly across the surface and that microstructural changes due to high-temperature exposure may have caused differences in local corrosion susceptibility. This phenomenon is likely caused by the precipitation of chromium carbides ($Cr_{23}C_6$) during prolonged exposure and slow cooling below the solution treatment temperature. This leads to chromium depletion near grain boundaries, which increases susceptibility to localized corrosion [34]. The slope of the trendlines quantitatively

Table 4. Average pit width (μm) and depth (μm) with corresponding trendline slopes for STS 304 and H_STS 304 after salt spray exposure at 200, 300, 400 and 500 hours

Specimen \ Spray Time		200 hours	300 hours	400 hours	500 hours	Slope
STS 304	Width	22.0	21.9	27.3	33.4	0.040
	Depth	2.6	2.8	3.4	6.1	0.011
H_STS 304	Width	22.0	26.7	36.2	45.7	0.081
	Depth	5.8	7.6	9.9	12.4	0.022

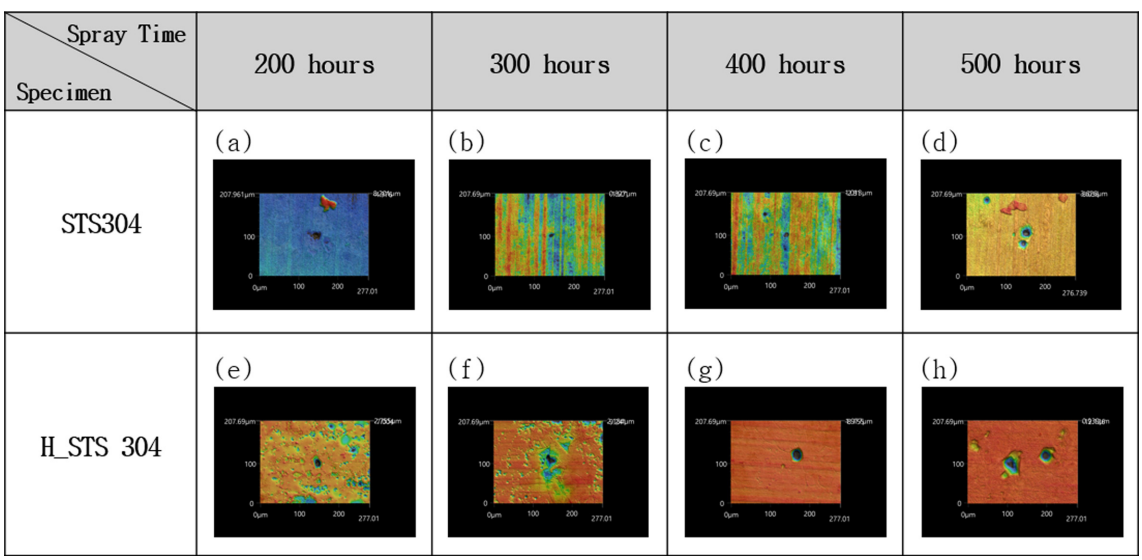

Fig. 6. Time-dependent 3D surface morphology of STS 304 and H_STS 304 specimens after the salt spray test: (a), (e) 200 hours, (b), (f) 300 hours, (c), (g) 400 hours, and (d), (h) 500 hours

represents the time-dependent rate of pit size increase and serves as an indicator for comparing localized corrosion progression between specimens. According to Table 4, the slope for pit width and depth in H_STS 304 was 0.081 μm/hour and 0.022 μm/hour, respectively. In contrast, STS 304 exhibited lower rates, with slopes of 0.040 μm/hour for width and 0.011 μm/hour for depth. These results indicate that pitting progressed more rapidly and severely in the heat-exposed specimens under identical exposure conditions. Therefore, the slope of the trendline can serve as a quantitative indicator of localized corrosion susceptibility. It also provides a practical metric for evaluating corrosion resistance degradation caused by high-temperature exposure.

Fig. 6 visually displays the pit morphology and distribution observed on the specimen surfaces using a 3D confocal laser scanning microscope. Compared to STS 304, the H_STS 304 specimens showed larger and more irregular pits distributed across a wider area. The localized concentration of pits observed in certain regions corresponds well with the broader variation and non-uniform distribution trends indicated in Fig. 4. These results suggest that the passive film was not uniformly maintained across the surface but instead experienced localized degradation. The 3D image analysis supports the non-uniform nature of localized corrosion revealed by the quantitative data.

4. Conclusions

In conclusion, the corrosion resistance of STS 304 austenitic stainless steel was shown to deteriorate following heat treatment, as confirmed by electrochemical polarization and salt spray tests. The H_STS 304 specimens exhibited lower corrosion potential (E_{corr}) and pitting potential (E_{pit}), along with unstable open-circuit potential (OCP) behavior, indicating reduced passive film stability. Three-dimensional surface profiling indicated that the H_STS 304 specimens had larger average pit sizes and greater variation in pit morphology, suggesting more severe and uneven localized corrosion. These findings align with previous studies attributing corrosion degradation to grain boundary sensitization caused by $Cr_{23}C_6$ precipitation. Therefore, components such as heat exchanger materials exposed to marine environments at elevated temperatures can exhibit significant susceptibility to corrosion depending on the applied heat treatment conditions.

Acknowledgments

This work was supported by a Research Grant of Gyeongkuk National University.

References

1. S. Y. Won, G. B. Kim, Y. R. Yoo, S. H. Choi, and Y. S. Kim, Intergranular Corrosion Behavior of Medium and Low Carbon Austenitic Stainless Steel, *Corrosion Science and Technology,* **21**, 230 (2022). Doi: https://doi.org/10.14773/cst.2022.21.3.230
2. ChaeEul Huh, and ChungSeok Kim, Microstructure and Corrosion Characteristics of Austenitic 304 Stainless Steel Subjected to Long-term Aging Heat Treatment, *Journal of the Korean Society of Manufacturing Process Engineers*, **21**, 56 (2022). Doi: https://doi.org/10.14775/ksmpe.2022.21.01.056
3. Saad R. Ahmed, Influence of high temperature on corrosion behavior of 304 stainless steel in chloride solutions, *AIP Advances*, **6**, 115310 (2016). Doi: https://doi.org/10.1063/1.4967204
4. U. J. Lim, B. D. Yun, and H. S. Kim, Effect of sensitization on the corrosion characteristics of STS 304 pipe, *Corrosion and Protection*, **6**, 9 (2007). Doi: https://doi.org/10.1016/j.ndteint.2017.02.007
5. D. IACOVIELLO. F. IACOVIELLO, and M. MACARIO, *IEEE 11th Mediterranean Conference on Control and Automation*, p. 1, IEEE, Rhodes, Greece (2003).
6. D. Iacoviello, F. Iacoviello, M. Macario, Neural networks application in an AISI 304L intergranular corrosion resistance analysis (2011).
7. Hong Pyo Kim, and Dong Jin Kim, Intergranular Corrosion of Stainless Steel, *Corrosion Science and Technology*, **17**, 183 (2018). Doi: https://doi.org/10.14773/cst.2018.17.4.183
8. H. S. Jeong, Z. G. Kim, and D. S. Um, A Study on the property and corrosion resistance of austenitic stainless base and weld metal, *Journal of Welding and Joining*, **14**, 71 (1996). https://koreascience.kr/article/JAKO199611919506674.pub
9. Eun-Jong Oh, Ph.D. Thesis, Pukyong National University, Busan (2020). https://libweb.pknu.ac.kr

10. Yong-Won Choi, Min-Su Han, and Seong-Jong Kim, Cavitation-erosion Resistance of Stabilized Stainless Steel with Niobium Addition in Sea Water Environment, *Journal of the Korean Institute of Surface Engineering*, **49**, 274 (2016). Doi: http://dx.doi.org/10.5695/JKISE.2016.49.3.274
11. Lingyun Bai, Wenyi Peng, Dandan Men, Jun Zhu, Xuecheng Wu, Xiongtao Shi, Junhuan Xiang, Xiaohua Deng, Yuqing Wang, Zuxiang Sun, Siqi Yu, and Xiang Wei, High Temperature Chloride Corrosion Behavior of 904L:AlFeNiMoNb High-Entropy Alloy, *Frontiers In Materials*, **8**, 1 (2021). Doi: https://doi.org/10.3389/fmats.2021.764928
12. Mohd Warikh Abd Rashid, Miron Gakim, Zulkifli Mohd Rosli, and Mohd Asyadi Azam, Formation of $Cr_{23}C_6$ During the Sensitization of AISI 304 Stainless Steel and its Effect to Pitting Corrosion, *International Journal of Electrochemical Science*, **7**, 9465 (2012). Doi: https://doi.org/10.1016/S1452-3981(23)16211-0
13. Qiaohui Sun, Fei Xie, Ying Zhang, Dan Wang, and Ming Wu, Stability of passive film and pitting susceptibility of 316 L stainless steel in the aggressive oilfield enviroment containing Cl^{-}-CO_2-O_2, *Electrochimica Acta*, **499**, 144709 (2024). Doi: https://doi.org/10.1016/j.electacta.2024.144709
14. S. Choudhary, R.G. Kelly, and N. Birbilis, On the origin of passive film breakdown and metastable pitting for stainless steel 316L, *Corrosion Science*, **230**, 111911 (2024). Doi: https://doi.org/10.1016/j.corsci.2024.111911
15. Hemalatha Parangusan, Jolly Bhadra, and Noora Al-Thani, A review of passivity breakdown on metal surfaces?influence of chloride- and sulfide-ion concentrations, temperature, and pH, *Emergent Materials*, **4**, 1187 (2021). Doi: https://doi.org/10.1007/s42247-021-00194-6
16. Zuocheng Wang, Antoine Seyeux, Sandrine Zanna, Vincent Maurice, and Philippe Marcus, Chloride-induced alterations of the passive film on 316L stainless steel and blocking effect of pre-passivation, *Electrochimica Acta*, **329**, 135159 (2020). Doi: https://doi.org/10.1016/j.electacta.2019.135159
17. Suwijak Pokwitidkul, Paweena Treewiriyakitja, Penpisuth Thongyoug, Nuntawat Kiatisereekul, Noparat Kanhanaprayut, and Hennarong Tungtrongpairoj, High temperature degradation of AISI 304L stainless steel in atomspheres containing CO of biomass to liquid plants at 800°C, *Materials Today: Proceedings*, **77**, 1100 (2023). Doi: https://doi.org/10.1016/j.matpr.2022.11.395
18. Xiaojia Yang, Menghao Liu, Zhiyong Liu, Cuiwei Du, and Xiaogang Li, Failure analysis of a 304 stainless steel heat exchanger in liquid sulfur recovery units, *Engineering Failure Analysis*, **116**, 104729 (2020). Doi: https://doi.org/10.1016/j.engfailanal.2020.104729
19. Kwang-Hu Jung, and Seong-Jong Kim, Efect of High Temperature Aging Time on Mechanical Characteristics Degradation of STS 304 Steel, *Journal of the Korean Institute of Surface Engineering,* **50**, 380 (2017). Doi: https://doi.org/10.5695/JKISE.2017.50.5.380
20. Piyanun Punburi, and Napachat Tareelap, Proper Heat Treatment to Reduce Intergranular Corrosion Susceptibility of Austenitic 304 and Ferritic 430 Stainless Steels, *Key Engineering Materials*, **545**, 143 (2013). Doi: https://doi.org/10.4028/www.scientific.net/KEM.545.143
21. Marcin Żuk, Artur Czupryński, Dariusz Czarnecki, and Tomasz Poloczek, The effect of niobium and titanium in base metal and filler metal on intergranular corrosion of stainless steels, *Welding Technology review,* **91**, 30 (2019). Doi: http://dx.doi.org/10.26628/wtr.v91i6.1032
22. Xun-zeng HUANG, Dan WANG, and Yi-tao YANG, Effect of Precipitation on Intergranular Corrosion Resistance of 430 Ferriric Stainless Steel, *Journal of iron and steel research, internarional,* **22**, 1062 (2015). Doi: https://doi.org/10.1016/S1006-706X(15)30113-8
23. Deepa Prabhu, Jilna Jomy and P.R. Parabhu, Influence of Different Heat Treatment Temperatures on the Microstructure and Corrosion Behaviour of Dual-Phase EN8 Steel in 0.5 M Sulphuric Acid Solution, *Journal of Bio- and Tribo-Corrosion*, **8**, 87 (2022). Doi: https://doi.org/10.1007/s40735-022-00689-7
24. J. O. Park, S. Matsch, and H. Böhni, Effects of temperature and chloride concentration on pit initiation and early pit growth of stainless steel, *Journal of The Electrochemical Society*, **149(2)**, B34–B39 (2002). Doi: https://doi.org/10.1149/1.1430415
25. Xingguo Feng, Tianyi Zhang, Ruihu Zhu, Zheng Chen, and Xiangyu Lu, Pitting initiation on 304 stainless steel in a chloride-contaminated pore solution under alternating temperature conditions, *Article in Corrosion Reviews*, **40**, 247 (2022). Doi: https://doi.org/10.1515/corrrev-2021-0070
26. Njoku Romanus Egwuinwu, Oblkwelu Daniel Nnamdi, Ugwuoke Benedeffe, and Ocheri Cyril, Investigation of Solution Annealing Treatment Effect on Corrosion Resistance of AISI 304 Austenitic Stainless Steel for Oil Industry Application, *Nanotechnology&Applications*, **6**, 1 (2023), https://www.scivisionpub.com
27. emitope Olumide Olugbade, and Babatunde Olamide Omiyale, Corrosion Resistance of Surface-Conditioned 301 and 304 Stainless Steels by Salt Spray Test, *Ana-*

lecta Technica Szegedinensia, **15**, 9 (2021). Doi: https://doi.org/10.14232/analecta.2021.2.9.-19

28. Steven R. Street, Markus Buchheit, and Jacob L. Hudson, The Effect of Deposition Conditions on Atmospheric Pitting Corrosion Location Under Evans Droplets on Type 304L Stainless Steel, *Corrosion*, **74**, 520 (2018). Doi: https://doi.org/10.5006/2614
29. C. Andrade, and C. Alonso, Test methods for on-site corrosion rate measurement of steel reinforcement in concrete by means of the polarization resistance method, *Materials and Structures*, **37**, 623 (2004). Doi: https://doi.org/10.1007/bf02483292
30. P. Panahi, S. N. Khorasant, R. A. Mensah, O. Das, and R. E. Neisiany, A review of the characterization methods for self-healing assessment in polymeric coatings, Progress in Organic Coatings, **186**, 108055 (2024). Doi: https://doi.org/10.1016/j.porgcoat.2023.108055
31. B. Elsener, and A. Rossi, Passivation of Steel and Stainless Steel in Alkaline Media Simulating Concrete, *Encyclopedia of Interfacial Chemistry Surface Sccience and Electrochemistry*, pp. 365 - 375, K. Wandelt, Elesvier, Amsterdam (2018). Doi: https://doi.org/10.1016/B978-0-12-409547-2.13772-2
32. P. W. Hang, B. S. Zhao, J. M. Zhou, and Y. Ding, Effect of Heat Treatment on Crevice Corrosion Behavior of 304 Stainless Steel Clad Plate in Seawater Environment, *Materials*, **16**, 3952 (2023). Doi: https://doi.org/10.3390/ma16113952
33. K. K. Lee, D. J. Yoon, W. B. Ghi, C. S. Kang, and D. J. Lee, An Oxidation Behavior with Heat-treatment in STS 304 and 316, *Journal of the Korean Society for Heat Treatment*, **11**, 186 (1998). https://koreascience.kr/article/JAKO199821757979314.page?&lang=en
34. H. K. D. H. Bhadeshia, and R. W. K. Honeycombe, *Steels: Microstructure and Properties, 3rd ed.*, p. 330, Elsevier, Amsterdam (2006). https://www.sciencedirect.com/book/9780750680844/steels?via=ihub=